ARCHIVES OF ACOUSTICS
9, 1-2, 143-154 (1984)

PROPERTIES OF HOLOGRAPHICALLY PRODUCED COMPLEX SPATIAL FILTERS FOR REAL-TIME DECONVOLUTION OF BLURRED ULTRASOUND IMAGES

JAN SOMER, FRANS JONGSMA

Medical Faculty, University of Limburg, Maastricht, The Netherlands

All ultrasound pulse-echo imaging systems suffer from limitations of both lateral and axial resolution due to beam-width and pulse-length respectively. Therefore a point-target will always be depicted as a blurred dot.

In essence only deconvolution of the system's impulse-response (or smear-function or blurring) could provide further improvement. Earlier an optical system was described potentially capable to process the echo-signals as received by a phased-array pulse-echo system in real-time and in two dimensions.

A holographic method can be used to produce a complex spatial filter for a particular reference-target which performs to some extent inverse filtering or deconvolution.

Both model-evaluations and experiments were carried out, showing a reasonable agreement.

With the used amplitude transmission-characteristic of the photographic emulsion complex spatial filters can be produced showing inverse-filter properties for only a small dynamic range.

Further work should be devoted to increasing the filter's dynamic range and dynamic range compression methods prior to the filtering.

1. Introduction

Previous publications [2-6] have already described how an optical computer can perform direct and quasi-inverse Fourier-transformation, and how filtering in the spatial frequency plane can be achieved.

Also, the conversion of the electrical signals, as received by the ultrasound phased-array system, into optically modulatable signals, employing an Ultrasound Light Modulator (ULM) was described.

Therefore, here we confine ourselves only to a description of the holographic procedure to produce a complex spatial "inverse" — filter and its performance.

2. The complex spatial filter

2.1. Holographic process

Already in 1964 VANDER LUGT published a method for producing a complex filter by means of a holographic process [1]. A holographic plate is illuminated by an object beam and a reference beam simultaneously, see Fig. 1. It is assumed that both beams originate from the same laser source in order to ensure the light

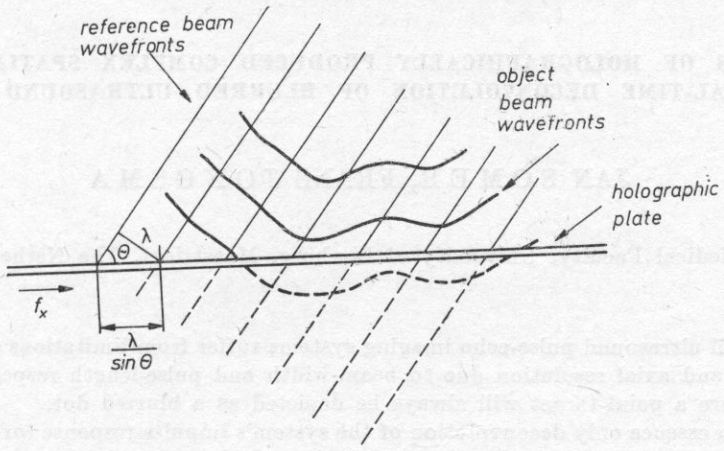

Fig. 1. Realization of a hologram

to be monochromatic and spatially and temporally coherent. Here, the object, beam is the spectrum $S_r(f_x, f_y)$ of the reference-target, of which both amplitude and phase are functions of f_x and f_y. The reference-target is a "point"-target, serving as a spatial δ-function input to the ultrasound system. At the surface of the holographic plate the complex function can be expressed as

$$\bar{S}_r = S_r(f_x, f_y) \exp\,[j\varphi(f_x, f_y)] = S_r \exp(j\varphi). \tag{1}$$

We require the reference beam to have a constant amplitude and an angle θ with the f_x — coordinate only.

It can be found from Fig. 1 that on the plate its complex amplitude can be described as

$$\bar{A}_r = A_r \exp(-j\alpha f_x) = A_r \exp(-j\psi), \tag{2}$$

where $\alpha = (2\pi \sin\theta)/\lambda$.

The total amplitude at the plate is now

$$\bar{A}_T = \bar{A}_r + \bar{S}_r = A_r \exp(-j\psi) + S_r \exp(j\varphi). \tag{3}$$

Since photographic emulsions respond to intensity, rather than to amplitude, we calculate the intensity, which is

$$I_T = \bar{A}_T \cdot \bar{A}_T^* = A_r^2 + S_r^2 + A_r S_r \exp[j(\psi+\varphi)] + A_r S_r \exp[-j(\psi+\varphi)] \tag{4}$$

$$= A_r^2 + S_r^2 + 2A_r S_r \cos(\psi+\varphi). \tag{5}$$

Equation (5) shows that the interference intensity-pattern consists of a "*DC*"-component (although S_r^2 is a variable) on which a modulation is superimposed, being proportional in amplitude with the object-beam and having a phase being the reference-beam phase which in its turn is modulated by the object-beam phase, since always $\varphi \ll \psi$. This illustrates that here in an intensity-function still both amplitude and phase are preserved, due to the use of a reference beam.

If the photographic emulsion would respond to the impinging light-energy such that the amplitude transmission of the developed plate would be a linear function of this energy, the amplitude transmission would also be expressed by equations ((4), (5)). An impinging reference-beam at zero angle would then fall apart into three beams as follows: $(A_r^2+S_r^2)$ at zero angle, and two beams proportional to S_r at angles $+\theta$ and $-\theta$, according to equation (2).

On the other hand, if in this special case the object-beam would impinge on the developed plate, the transmitted beams would be proportional to:

a. $(A_r^2+S_r^2)S_r\exp(j\varphi)$, being a distorted object beam at "zero" angle

b. $S_r^2\exp[j(\psi+2\varphi)]$, being the squared amplitude object-beam with distorted phase at an angle $+\theta$.

c. $S_r^2\exp(-j\psi)$, being again the squared amplitude object-beam with cancelled phase under an angle $-\theta$.

2.2. Holographic "inverse" filter

In [4, 5, 6] it was pointed out that the filter should have a transfer-function,

$$\bar{G} = 1/\bar{S}_r = 1/(S_r\exp(j\varphi) = (1/S_r)\exp(-j\varphi). \tag{6}$$

In paragraph 2.1 it was found that in the $(-\theta)$-diffraction component of the hologram this negative phase is present (leading to the phase-cancellation as in case *c*), so this aspect is correct. However, instead of $1/S_r$, the amplitude transfer-function of the hologram in 2.1 is S_r so that to obtain an inverse filter the amplitude transmission-function of the holographic plate as a function of the exposure energy should definitely not be linear as was assumed in 2.1.

Fig. 2 shows a realistic amplitude transmission curve T_a as a function of $E = It$, the exposure-energy, with t = exposure-time. It also shows the intensity-function according to equation (5). Here, S_r runs linearly from 0 to 1 and the ratio $A_r/S_{r\max}$ is less than 1. Due to the very non-linear T_a-curve a high modulation-amplitude causes a low transmission-modulation and reversed.

Qualitatively this is just what we wish to achieve. However, to which extent the obtained transmission-modulation function approximates the actually wanted $1/S_r$ (according to equation (6)), will be investigated further.

2.3. Evaluation of a model

The result as shown in Fig. 2 suggests that, given a particular T_a-E function, the two possible parameters which can be varied are the beam-amplitude

ratio

$$R_a = A_r/S_{r\max} \tag{7}$$

and the T_{aDC}-value, being the transmission corresponding to the maximum *DC*-component value, see Fig. 2.

Alteration of R_a causes considerable variation of the *DC*-component as a function of S_r. The T_{aDC}-value can be adjusted by proper estimation of the exposure-time t.

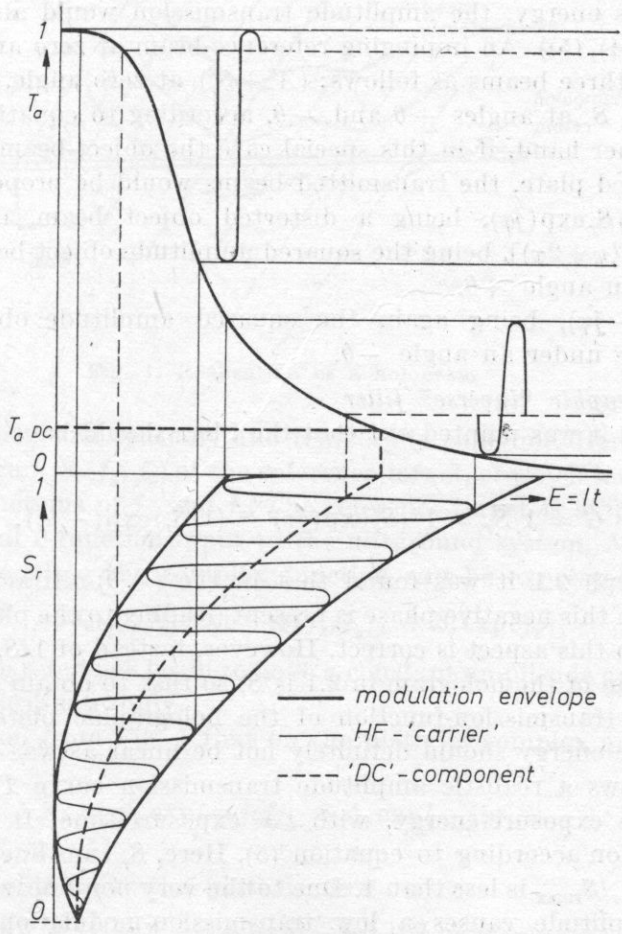

Fig. 2. Realization of a complex spatial "inverse" filter

The process as shown in Fig. 2 can be investigated further by fitting the measured T_a-curve of a particular type of photographic material under particular development-conditions by a mathematical function $T_a(E)$.

The exposure-energy E can be found from equations (5) and (7), together

with stating that $S_{r\max} = 1$ (for convenience), as follows

$$E = It = \{R_a^2 + S_r^2 + 2R_a S_r \cos(\psi + \varphi)\}t, \tag{8}$$

where t = exposure-time.

In practice θ, the angle of the reference beam, is always taken large enough to let $\psi = \alpha f_x = (2\pi \sin\theta \cdot f_x)/\lambda$ (see equation (2)) be much greater then φ (equation (1)). The modulation frequency, therefore, is mainly determined by ψ and is very close to $(\sin\theta)/\lambda\varphi$ and in our case approximately 100 cycles per millimeter.

Since for this model the phase of the spectral function S_r is assumed to be zero (again for convenience), we can write

$$E = \{R_a^2 + S_r^2 + 2R_a S_r \cos\psi\}t, \tag{9}$$

with

$$\psi = 2\pi\ 100\ f_x, \tag{10}$$

where f_x is measured in mm on the holographic plate.

Substitution of equation (9) into $T_a(E)$ yields

$$T_a = T_a(\psi), \tag{11}$$

with the parameters R_a as the beam-amplitude ratio, S_r as the spectral amplitude of the input-function to the system and t as the exposure-time to obtain the required T_{aDC}-value.

From Fig. 2 we will appreciate that the original cosine-function of equation (9) is highly distorted by the non-linear $T_a - E$ characteristic, resulting in an oscillating function with many harmonics ψ, 2ψ, 3ψ etc.

Illuminated by a beam this grating pattern will accordingly split it up in diffractions at $+\theta$ and $-\theta$, $+2\theta$ and -2θ, $+3\theta$ and -3θ, etc. In using such a grating as a complex spatial filter only the first order diffraction at $-\theta$ is selected out.

In our mathematical model we assume that S_r varies very slowly with the co-ordinate f_x, which means that at every position f_x the spectral amplitude S_r can be considered to be constant over several grating-oscillations. This makes $T_a(\psi)$, as represented by equation (11), a periodic function with ψ as the only variable and thus $T_a(\psi)$ can be expressed as a Fourier-series

$$\begin{aligned} T_a(\psi) &= A_0 + A_1 \cos\psi + A_2 \cos 2\psi + \ldots \\ &= A_0 + \frac{A_1}{2}\left(\exp(j\psi) + \exp(-j\psi)\right) + \frac{A_2}{2}\left(\exp(j2\psi) + \exp(-j2\psi)\right) + \ldots \end{aligned} \tag{12}$$

As mentioned above, we are interested in the first order $(-\theta)$-diffraction only so that we merely have to evaluate A_1.

From Fourier-series theory we calculate

$$A_1 = \frac{1}{\pi} \int_{-\pi}^{+\pi} T(\psi) \cos \psi d\psi \tag{13}$$

for several values of S_r. Herewith we in fact obtain A_1 and thus G as a function of the spectral amplitude S_r, still with R_a and T_{aDC} as parameters.

One should realize that we did not find the transfer-function $G(f_x)$ in the spatial-frequency plane of the holographic complex spatial filter for a spectrum S_r, unless $S_r(f_x)$ is defined.

If for all frequencies $G(f_x) = 1/S_r(f_x)$, which is required for an inverse filter equation (6), then $G(f_x)S_r(f_x) = 1$.

Accordingly, A_1S_r should be constant for all S_r. We can now determine the product of spectral amplitude and filter-function as a function of the spectral amplitude, in other words

$$A_1S_r = f(S_r). \tag{14}$$

The range of S_r over which A_1S_r is "constant" (within certain limits) then determines the maximum dynamic range of S_r for which the used T_a-E curve can produce a suitable inverse filter.

In Fig. 3*a*, *b*, *c* the model calculations are presented for $R_a = 2/3$, 1/2 and 1/3 respectively. Four curves are given representing four different T_{aDC}-values, according to Table 1. In Table 1 the dynamic ranges of S_r are also given for all cases (as far as applicable) within 3 dB and 6 dB limits respectively. The first conclusion is that the dynamic ranges are very small and more dependent on T_{aDC} than on R_a.

Further comments will be given in the next chapter.

2.4. Experiments

For confirmation of the model found, a number of experiments were carried out. A grey-wedge with a continuously and logarithmically varying density over a range of approximately 30 dB, was used for creating the function $S_r(f_x)$.

Holograms were made under conditions defined as well as possible with respect to R_a, T_{aDC} and a high enough oscillating frequency of the grating-pattern.

Each hologram was illuminated with the same spectral distribution $S_r(f_x)$ as used for creating the hologram with accurately co-inciding f-scales. Then the $(-\theta)$-diffraction was recorded (corresponding with A_1 in the previous chapter), together with the spectral distribution $S_r(f_x)$ itself. The data were processed by a computer and f_x was eliminated in order to obtain A_1S_r as a function of S_r, similarly to the model-evaluation in the previous chapter (equation (14)).

The results are given in Fig. 4 *a*, *b*, *c* in combination with Table 2.

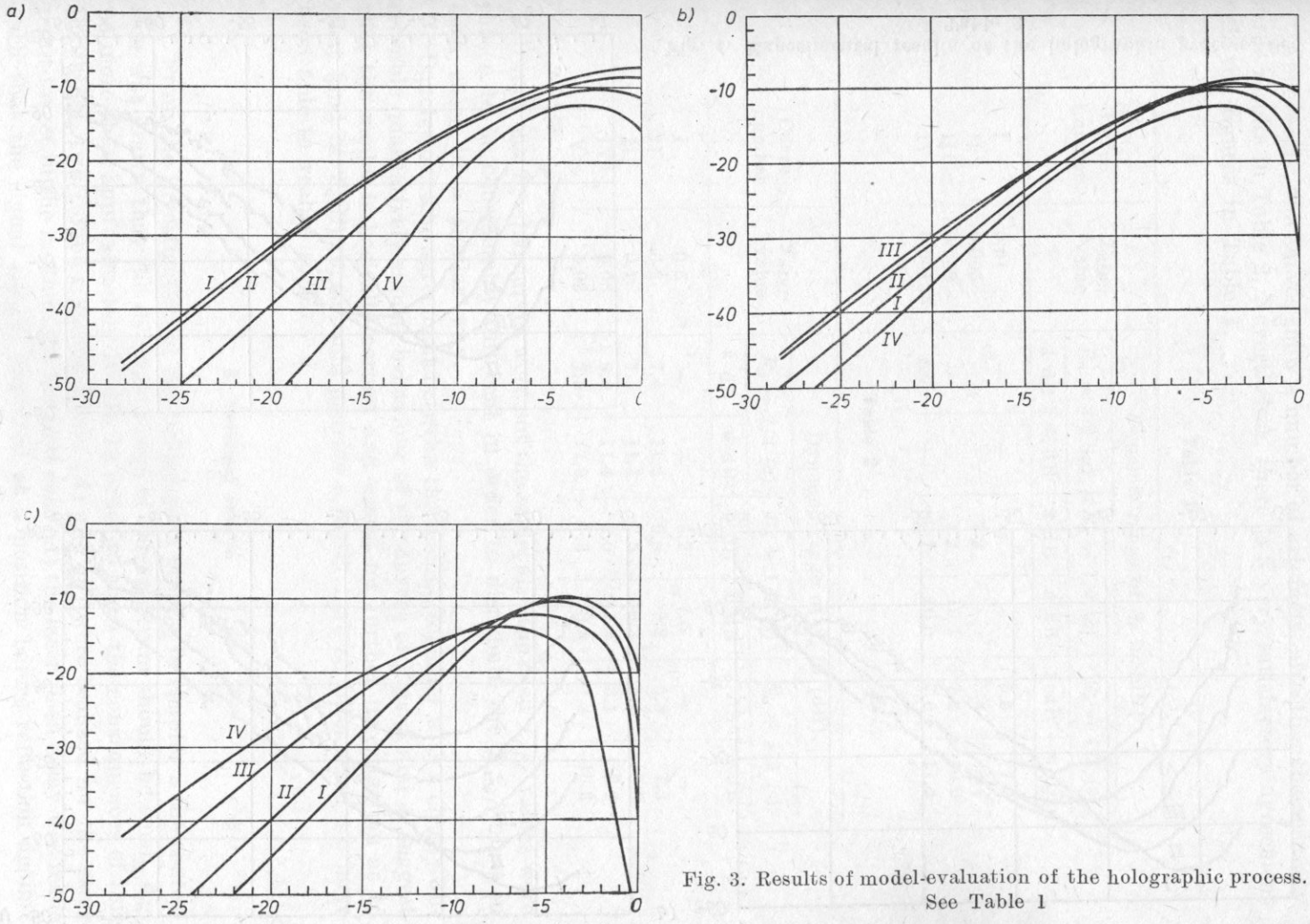

Fig. 3. Results of model-evaluation of the holographic process. See Table 1

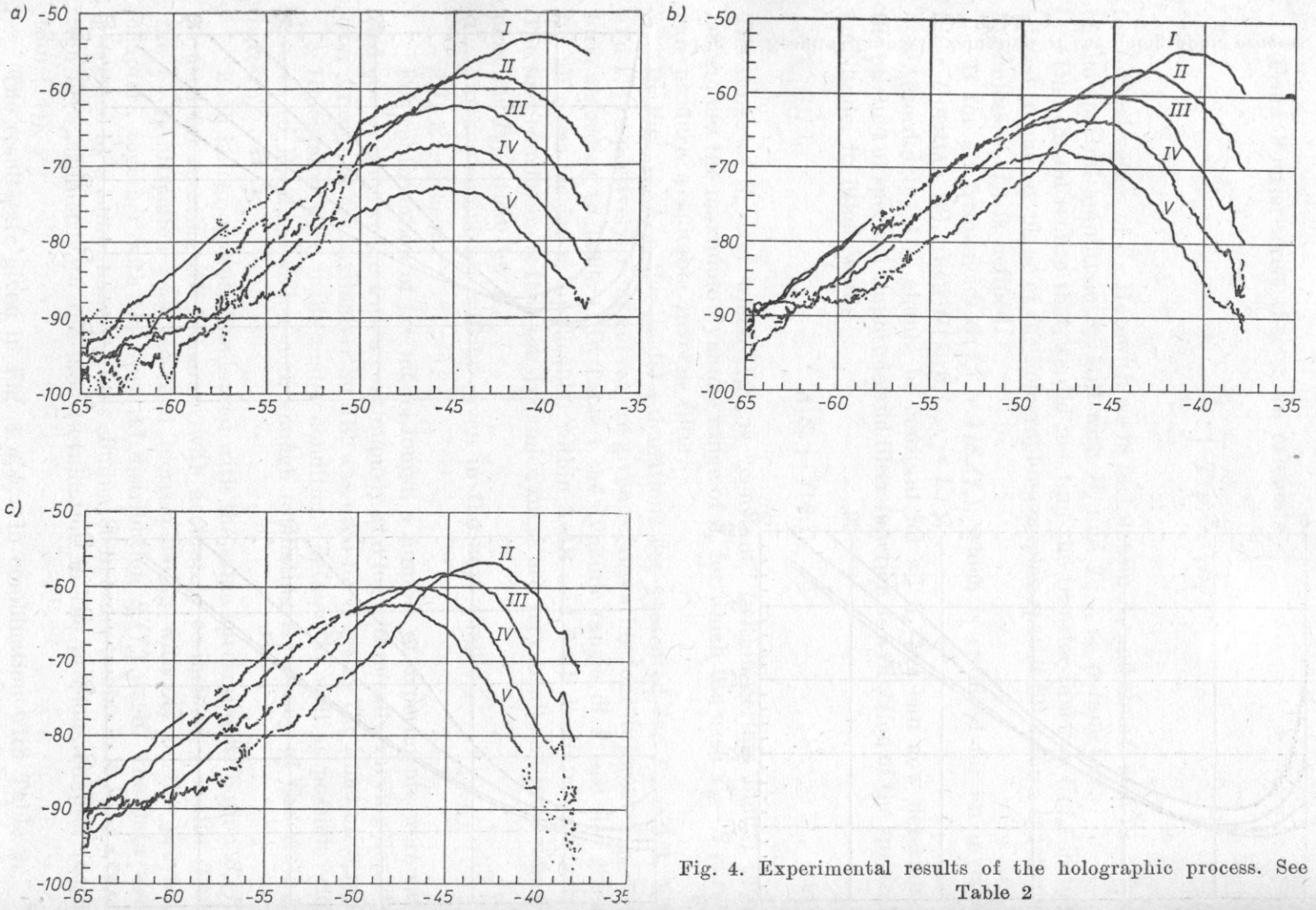

Fig. 4. Experimental results of the holographic process. See Table 2

Apparently, the curves show a number of artefacts, affecting the accuracy of the results in Table 2. Nevertheless, there is a very satisfactory agreement with the figures in Table 1.

Table 1

Curve number	T_{aDC}-value	Dynamic range of S_r in [dB]					
		$R_a = 2/3$ (*a*)		$R_a = 1/2$ (*b*)		$R_a = 1/3$ (*c*)	
		3 dB	6 dB	3 dB	6 dB	3 dB	6 dB
I	0.01	–	–	–	–	5.5	7.9
II	0.005	–	–	7.2	–	5.8	8.4
III	0.002	–	–	7.2	10.7	7.2	10.0
IV	0.00135	6.7	–	7.1	10.0	7.6	11.2

Table 2

Curve number	T_{aDC}-value	Dynamic range of S_r in [dB]					
		$R_a = 2/3$ (*a*)		$R_a = 1/2$ (*b*)		$R_a = 1/3$ (*c*)	
		3 dB	6 dB	3 dB	6 dB	3 dB	6 dB
I	0.5	–	–	5.2	7.5	–	–
II	0.2	7.4	11.2	5.8	9.2	5.3	7.3
III	0.1	7.5	11.4	7.5	10.3	5.4	8.0
IV	0.05	8.0	11.4	8.0	11.4	6.1	9.2
V	0.02	7.5	11.0	7.3	10.8	7.3	10.3

Since the $T_a-(E)$ curves were not the same, also the used T_{aDC}-values were chosen to be considerably different in order to distribute the T_{aDC}-values in both cases in a similar way.

Conclusion: The agreement between the results, together with a clearly observable qualitatively similar behaviour of the curves of Figs. 3 and 4, suggest that the model is basically correct and useful for further investigation as to what kind of $T_a(E)$-curve could provide a better inverse filter than we have been able to realize so far.

3. Practical results

From the investigation of the holographic process in chapter 2 the conclusion was drawn that the dynamic range of the spectrum should be small, e.g. no more than approximately 10 dB. In order to show the consequences of this limitation, two complex spatial filters (*A*) and (*B*) were realized for the same point-target in the medium. In the first case (*A*) the laser-flash delay was made such that the signal $s_r(x, y)$ appeared at a position before reflection against

the paraboloid reflector, whereas the second case (B) was the normal situation with the signal $s_r(x, y)$ shown after reflection.

Obviously the flattening of the wave-fronts at reflection against the paraboloid reflector causes a considerable increase of power-concentration through the Fourier-transformation.

Fig. 5 shows case (A) with respectively the obtained spectrum (a), the unfiltered signal supposed to be identical to $s_r(x, y)$ in the input plane (b) and zero and first diffraction orders in the output plane (c).

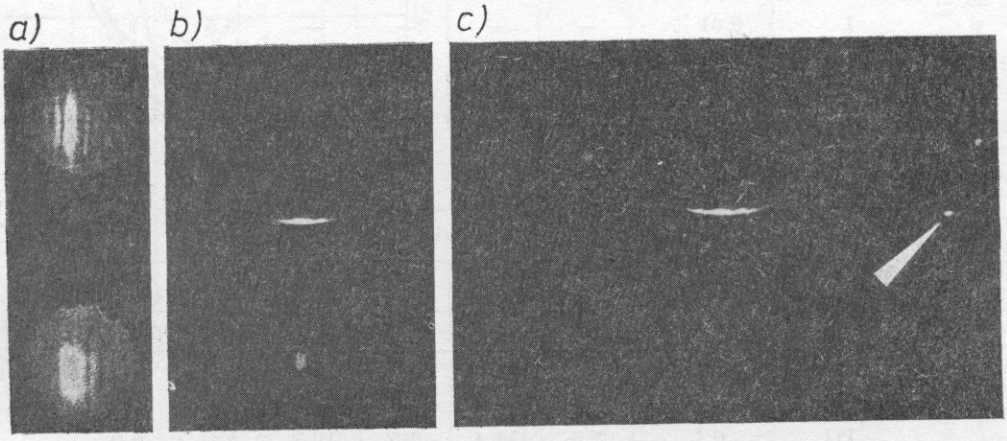

Fig. 5. Practical results for non-reflected signals

As explained in 2.3, the filter-result appears as the $(-\theta)$-diffraction and is indicated by an arrow in Fig. 5c.

Apparently, a very effective deconvolution has been obtained since this very small spot is depicted at the same scale as $s_r(x, y)$ in (b).

Fig. 6 represents results obtained in case (B). In (a) five signals are shown as they appeared unfiltered in the output plane, again supposed to be identical to the input-signals. The scanned object consisted of five "point"-targets in a rhombus-shaped configuration and the image shows clearly the position-deformation caused by the paraboloid reflector. A filter was realized with only the center-target present in the medium and after installing the filter the corner-targets were mounted at their positions. In Fig. 6b we see the filter-results, being much less spectacular than in case (A). In Fig. 6c and d the signals are shown as measured quantitatively.

It is clear that the gain in spatial invariance by using a paraboloid reflector (as a proof showing the five filtered signals in Fig. 6b as being quite similar) has been obtained at the expense of filter-performance because of the increased dynamic range of the spectra. Everything is in good agreement with the results of the model-investigation in chapter 2.

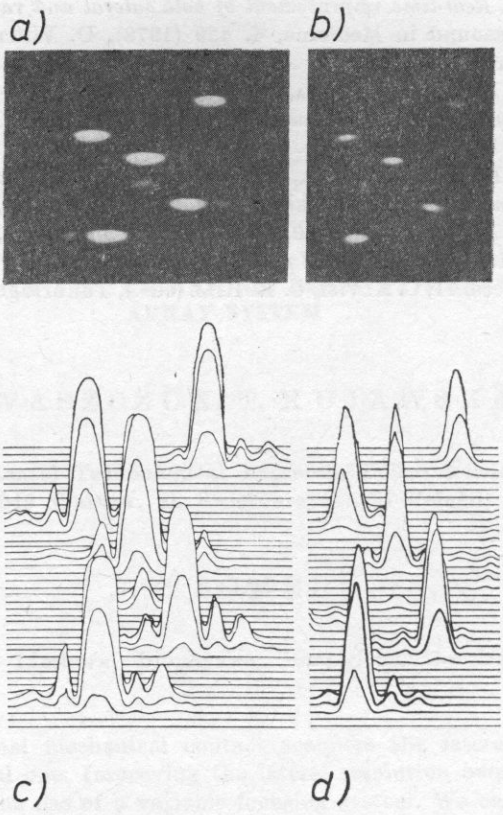

Fig. 6. Practical results for signals after reflection

8. Conclusions

With a complex spatial filter in the spatial frequency plane of an optical computer filtering can be performed. A holographic method has been described to realize such a filter which acts as an inverse filter provided that the spectrum to be processed has a small dynamic range.

Both increasing dynamic range of the filter and compression of the spectrum's dynamic range are the goals of further investigations.

References

[1] A. Vander Lugt, *Signal detection by complex spatial filtering,* IEEE Trans. on Information Theory, IT-10, 139 (1964).

[2] J. C. Somer, *Real-time improvement of both lateral and range resolution by optical signal processing,* 1977 Ultrasonics Symposium Proceedings, **77CH**-1264-1 SU, New York, IEEE 1002.

[3] J. C. SOMER, *Real-time improvement of both lateral and range resolution by optical signal processing,* Ultrasound in Medicine, **4**, 439 (1978), D. WHITE, E. A. LYONS (eds.), New York, Plenum Press.

[4] J. C. SOMER, E. H. M. JONGSMA, W. L. J. MARTENS, *Real-time two-dimensional resolution improvement by optical signal processing,* Proc. UBIOMED IV 1979, **1**, 14, P. GREGUSS, (ed.), Visegrad, Hungary.

[5] J. C. SOMER, E. H. M. JONGSMA, W. L. J. MARTENS, *Application of an acousto-optic device in an optical deconvolver for blurred ultrasound-diagnostic images,* Proc. 1st Spring School on Acoustooptics and Applications, 1980, 202, Gdańsk University, Physics Institute.

[6] J. C. SOMER, 1980. *Optical signal processing in ultrasound,* Investigative Ultrasonology, **1**, Technical Advances, 71, C. ALVISI, C. R. HILL (eds.), Tunbridge Wells, Pitman Medical, 1980.